Pergamon

Acta mater. Vol. 45, No. 11, pp. 4823–4834, 1997

PII: S1359-6454(97)00098-0
1359-6454/97 $17.00 + 0.00

MODELLING VISCOPLASTIC BEHAVIOR OF ANISOTROPIC POLYCRYSTALLINE ICE WITH A SELF-CONSISTENT APPROACH

O. CASTELNAU[1]†, G. R. CANOVA[2], R. A. LEBENSOHN[3] and P. DUVAL[4]

[1]LPMTM-CNRS, Université Paris-Nord, Institut Galilée, av. J.B. Clément, 93430 Villetaneuse, [2]GPM2-ENSPG, Domaine Universitaire, 38402 St. Martin d'Hères Cedex, France, [3]Instituto de Fisica Rosario (UNR-CONICET), 27 Febrero 210 bis, 2000 Rosario, Argentina and [4]LGGE-CNRS, Domaine Universitaire, 38402 St. Martin d'Hères Cedex, France

(Received 31 October 1996; accepted 24 December 1996)

Abstract—A ViscoPlastic Self-Consistent (VPSC) model has been applied to polycrystalline ice in order to characterize the relation between the texture of the material and the instantaneous anisotropic mechanical behavior. We assume that ice crystals deform by basal, prismatic, and pyramidal slip. The resistance of these slip systems is determined by an inverse approach, based on the comparison between model results and results of several mechanical tests. The VPSC model well reproduces all experimental macroscopic behavior only if we introduce a small—but not negligible—amount of pyramidal slip, which is not observed experimentally. The introduction of this probably unrealistic slip system possibly corrects the errors linked to the assumptions of the model, that we discuss. We finally use the model to describe the behavior of some typical polar ices in relation to the symmetries of the texture. © *1997 Acta Metallurgica Inc.*

Résumé—On applique un modèle autocohérent viscoplastique (VPSC) à la glace polycristalline dans le but de caractériser la relation entre la texture du matériau et son comportement mécanique anisotrope instantané. On suppose que les grains de glace se déforment par glissement basal, prismatique, et pyramidal. La résistance de ces systèmes de glissement est déterminée par une méthode inverse basée sur la comparaison des résultats du modèle à ceux d'essais mécaniques. On montre que le modèle VPSC permet de bien reproduire les comportements macroscopiques expérimentaux seulement si l'on introduit une activité pyramidale faible—mais non négligeable—qui n'est pas observée expérimentalement. L'introduction de ce système de glissement probablement irréaliste pourrait être une manière de corriger les erreurs liées aux hypothèses du modèle, que l'on discute. On utilise enfin le modèle pour décrire le comportement mécanique de glaces polaires typiques en relation avec les symétries de la texture.

1. INTRODUCTION

Ice from polar ice sheets (like Greenland and Antarctica) is a viscoplastic polycrystalline material that presents a hexagonal crystalline structure (ice Ih). Like most hexagonal materials, ice crystals exhibit a very large viscoplastic anisotropy. Only basal glide significantly contributes to the deformation, and less than five independent slip systems are expected. Polar ices present interesting characteristics compared to other classical polycrystalline materials: (i) the content of soluble impurities is very low, generally less than 1 μm/g, (ii) grain size is large, typically 10 mm^2, and (iii) twinning is not an active deformation mechanism.

Observations of deep ice cores have revealed the presence of preferred lattice orientations (texture). At the surface of the ice sheet, ice presents a randomly oriented texture, and is thus macroscopically isotropic. But with increasing depth, a concentration of c-axes around the *in situ* vertical direction is generally found, e.g. in the Law Dome (Antarctica) and GRIP (Greenland) ice cores [1, 2]. A more particular texture with c-axes aligned in a vertical plane was found in the Vostok (Antarctica) core [3]. As long as the temperature is lower than -12°C, these textures mainly develop as a result of the plastic deformation due to intracrystalline dislocation glide.

In this work, we deal with the strong viscoplastic anisotropy induced by these textures, and we concentrate on the relation between texture and instantaneous mechanical behavior. Anisotropy of textured ice polycrystals has been largely studied experimentally, e.g. see [4–6]. For a given equivalent stress, the deformation rate can differ by more than two orders of magnitude for the same sample, depending on the direction of the prescribed stress. The flow of ice sheets, which must be accurately modelled to obtain a better understanding of past Earth climates, is significantly influenced by this anisotropy [7, 8]. Ice flow models must thus take into account an anisotropic constitutive relation formu-

†To whom all correspondence should be addressed.

lated in large deformations. However, the analytical constitutive relations developed up to now for anisotropic polar ices [9, 10] have never been completely tested on experiments nor on *in situ* measurements.

In this work, we apply the Visco-Plastic Self Consistent (VPSC) model to polar ice in order to estimate numerically the behavior of polycrystals exhibiting a given (fixed) texture, i.e. in the case of small deformations. The VPSC approach, first developed by Hutchinson [11], formulated in an alternative framework by Molinari *et al.* [12], and applied to macroscopically anisotropic materials by Lebensohn and Tomé [13], can be used to derive, according to the active deformation mechanisms, an interaction equation that links microscopic states (stress and strain rate at the grain or subgrain scales) with the macroscopic state (at the polycrystal scale). A first order solution (the so-called "1-site scheme") of the incompressibility and stress equilibrium equations applied over the entire polycrystal volume is obtained when the interaction between neighboring grains is not directly considered, but when each grain is successively considered as an ellipsoidal inclusion in a Homogeneous Equivalent Medium (HEM) whose behavior represents that of the polycrystal. This treatment allows the stress and strain rate to be different in each grain. The first applications of this VPSC model to calculate texture development in ice were presented by Castelnau *et al.* [14, 15].

A limitation of this homogenization method is that a constitutive relation must be assumed for the grains. This means that once a particular form of this relation has been chosen, it is necessary to find physically reasonable values of all microscopic parameters that provide acceptable results at the microscopic and macroscopic scales. One method consists of adjusting microscopic parameters on the rheology measured on *isolated* single crystals. This treatment presents the advantage of being very simple, but it is *a priori* not satisfactory. Indeed, the behavior of crystals should depend on the ability of crystal boundaries to produce and to absorb mobile dislocations [16]. However, crystal boundaries can present different structures, e.g. a grain boundary for a polycrystal and a free surface for an isolated single crystal. The flow stress of an *in situ* grain, i.e. of a grain within a polycrystal, would therefore be expected to be different from that of an isolated single crystal. Other methods, such as those recently proposed by Mercier *et al.* [17] and Tóth and Serghat [18], are based on the comparison between model results and experimental macroscopic stress–strain curves associated with texture development or active slip systems observed in grains having different orientations. These methods are not suitable for ice, as such experimental data, to our knowledge, are not available at present. In previous applications of the VPSC model to polar ice [14, 15], basal and non-basal resistances of *in situ* grains were adjusted to minimize non-basal activities and to reproduce the viscosity of an *isotropic* polycrystal. The obtained values of slip resistances were sufficiently accurate to study texture development, but not to evaluate the rheology of anisotropic samples. Indeed, the macroscopic behavior of strongly textured polycrystals significantly depends on not well known values of non-basal resistances. We present here a different approach, based on an inverse method, for finding these microscopic parameters.

The aim of this work is to analyze how the texture of the material influences the instantaneous macroscopic mechanical behavior. After a brief review of ice rheology (Section 2) and VPSC formulation (Section 3), we present the method we used to obtain the microscopic parameters (Section 4). We look for all possible sets of slip resistances that accurately reproduce the instantaneous behavior of several *anisotropic* polycrystals. For the VPSC model, we find one set of microscopic parameters that accurately reproduces *in average* experimental data. The classical Voigt-type upper bound (Taylor model, uniform strain rate within the polycrystal) and Reuss-type lower bound (static model, uniform stress) are also used here. Both bounds give very different results when the microscopic anisotropy is large, and the comparison between VPSC, Taylor, and static models shows that microscopic parameters are very sensitive to model assumptions: slip resistances determined with the VPSC model are one order of magnitude lower than those obtained with the static model. In the second part of the paper (Section 5), we use the obtained values of slip resistances to highlight some important features of the behavior of strongly textured ice polycrystals. We find a very good agrement between VPSC results and *all* experimental data, and we show in particular how slight deviations in texture symmetries may influence the macroscopic behavior. The discussion focuses on some limitations of the VPSC formulation for non-linear and very anisotropic materials, and on precautions that must be taken when performing mechanical tests on anisotropic ices.

2. BEHAVIOR OF MONOCRYSTALLINE AND ISOTROPIC POLYCRYSTALLINE ICE

The main feature of the plasticity of ice crystals is its outstanding anisotropy. Almost all dislocation lines observed in ice Ih lie in the basal plane $\{0001\}$, with the three $(a/3)\langle 2\bar{1}\bar{1}0\rangle$ Burgers vectors [19]. As a result of the low stacking fault energy, basal dislocations are generally dissociated, which impedes their cross slip on non-basal planes [20–22]. Non-basal dislocations are observed in the form of very short edge segments. They have a basal Burgers vector, and their slip plane should lie between the $\{\bar{1}010\}$ and $\{\bar{1}012\}$ planes [23, 22]. Due to their very short length, these edge segments cannot contribute significantly to the total deformation of grains. In

addition, dislocations in which the Burgers vector has a [0001] component are expected. However, there is no evidence that these dislocations can glide, i.e. that ice crystals can deform plastically by slip in the direction of the *c*-axis [24]. Therefore, ice crystals should present less than five independent slip systems.

According to Duval *et al.* [25], the deformation rate of single crystals deformed by basal glide is at least four orders of magnitude larger, for a given prescribed stress, than that obtained when only non-basal systems are activated. The steady state behavior of ice crystals is well represented by the classical relation proposed by Hutchinson [11]:

$$\dot{\gamma}^s = \dot{\gamma}_0 \left| \frac{\tau_r^s}{\tau_0^s} \right|^{n^s - 1} \frac{\tau_r^s}{\tau_0^s}, \tag{1}$$

where $\dot{\gamma}^s$ is the shear rate on the slip systems s, and $\dot{\gamma}_0$ is a reference shear rate taken equal to unity ($\dot{\gamma}_0 = 1\ s^{-1}$). The stress exponent n^s and the Reference Resolved Shear Stress (RRSS) τ_0^s are the parameters of this constitutive relation. The resolved shear stress τ_r^s on the system s is given by:

$$\tau_r^s = \mathbf{r}^s : \mathbf{S}, \tag{2}$$

where $\mathbf{S}$ is the deviatoric Cauchy stress tensor and ":" indicates the twice contracted tensorial product. The Schmid tensor $\mathbf{r}^s$ depends on the orientation of the system s relative to the reference frame:

$$\mathbf{r}^s = \tfrac{1}{2}(\mathbf{n}^s \otimes \mathbf{b}^s + \mathbf{b}^s \otimes \mathbf{n}^s) \tag{3}$$

where $\mathbf{n}^s$ and $\mathbf{b}^s$ are unit vectors normal to the slip plane and parallel to the Burgers vector, respectively. The strain rate tensor then reads:

$$\mathbf{D} = \sum_s \dot{\gamma}^s \mathbf{r}^s. \tag{4}$$

In monocrystalline ice, the generally adopted value for the basal stress exponent is $n^{\text{basal}} = 2 \pm 0.2$ [25]. The value of non-basal exponents is not well defined, but seems to be close to 3.

The secondary creep of *isotropic* polycrystalline ice is reached for a strain of about 1%. This stage is generally considered as corresponding to the "steady state" behavior. It is well represented by the Norton relation, also called "Glen flow law" in Glaciology [25]:

$$\bar{\mathbf{D}} = \frac{3}{2} \dot{\gamma}_0 \frac{\bar{S}_{eq}^{n-1}}{\sigma_0^n} \bar{\mathbf{S}}. \tag{5}$$

Here, $\bar{S}_{eq}$ is the equivalent stress defined as $\bar{S}_{eq} = (3 \times \bar{\mathbf{S}} : \bar{\mathbf{S}}/2)^{1/2}$. The macroscopic stress exponent n is equal to 3 for strain rates larger than about $10^{-9}\ s^{-1}$. The macroscopic reference stress σ_0 is temperature dependent. Its value slightly depends on the kind of ice and on the experimental test conditions. It is estimated to be equal to 234 MPa ± 25% at $-10°C$ according to the experimental results of Budd and Jacka [6].

3. THE VPSC FORMULATION

We will briefly review in this section the main equations of the "1-site" VPSC model. More details can be found in Molinari *et al.* [12] and in Lebensohn and Tomé [13]. This model consists of replacing successively the interaction between an *in situ* grain and its surrounding by the interaction between a grain of the same lattice orientation and an infinite HEM. The related inclusion problem can be solved by an extension of the classical Eshelby [26] formalism to viscoplastic materials only if the behavior of the HEM is linear. As a result, stress and strain rate are found to be uniform in each grain if grain shape is assumed to be ellipsoidal. The stress $\bar{\mathbf{S}}$ and strain rate $\bar{\mathbf{D}}$ prescribed on the polycrystal surfaces are assumed to be uniform, and are linked by the following non-linear constitutive relation:

$$\bar{\mathbf{D}} = \mathbf{M}^{(sec)} : \bar{\mathbf{S}}. \tag{6}$$

The secant compliance tensor $\mathbf{M}^{(sec)}$ is a homogeneous function of degree $n - 1$ of the stress and is structure dependent. The behavior of the HEM is approximated by a first order Taylor expansion of equation (6) in the vicinity of $\bar{\mathbf{S}}$:

$$\mathbf{D} = \mathbf{M}^{(tg)}(\bar{\mathbf{S}}) : \mathbf{S} + \mathbf{D}^0(\bar{\mathbf{S}}), \tag{7}$$

where the tangent compliance $\mathbf{M}^{(tg)}$ is given by:

$$M_{ijkl}^{(tg)}(\mathbf{S}) = \frac{\partial D_{ij}}{\partial S_{kl}}(\mathbf{S}). \tag{8}$$

In equation (7), $\bar{\mathbf{S}}$ and $\bar{\mathbf{D}}$ designate the stress and strain rate at infinity in the HEM, and $\mathbf{S}$ and $\mathbf{D}$ the same quantities locally in the HEM. Secant and tangent compliances are proportional:

$$\mathbf{M}^{(tg)} = n\mathbf{M}^{(sec)} \tag{9}$$

if all microscopic stress exponents n^s are equal, in which case $n = n^s$. The extension of the Eshelby inclusion problem to viscoplastic materials leads to the following interaction equation, which relates microscopic and macroscopic states:

$$\mathbf{D}^g - \bar{\mathbf{D}} = -\tilde{\mathbf{M}} : (\mathbf{S}^g - \bar{\mathbf{S}}), \tag{10}$$

where the exponent g designates a particular grain. The interaction tensor $\tilde{\mathbf{M}}$ depends on the macroscopic compliance and on the shape of the grains (here assumed to be spherical). This allows the stress and strain rate to be different in each grain. If a stress localisation tensor $\mathbf{B}^g$ is defined by the relation:

$$\mathbf{S}^g = \mathbf{B}^g : \bar{\mathbf{S}}, \tag{11}$$

then $\mathbf{B}^g$ reads:

$$\mathbf{B}^g = (\mathbf{M}^{g(sec)} + \tilde{\mathbf{M}})^{-1} : (\mathbf{M}^{(sec)} + \tilde{\mathbf{M}}) \tag{12}$$

where the microscopic compliance $\mathbf{M}^{g(sec)}$ is defined

Table 1. Slip family, number of independent systems per family, and reference resolved shear stress

		Nb. Syst.	RRSS
Basal	$\{0001\}\langle 11\bar{2}0\rangle$	2	τ_b
Prismatic	$\{01\bar{1}0\}\langle 2\bar{1}\bar{1}0\rangle$	2	τ_{pr}
Pyramidal	$\{11\bar{2}2\}\langle 11\bar{2}\bar{3}\rangle$	5	τ_{py}

from equation (4) by the relation:

$$\mathbf{D}^g = \mathbf{M}^{g(sec)}:\mathbf{S}^g. \tag{13}$$

The solution is found when the volume integral (denoted "$\langle . \rangle$") of the microscopic states equals the macroscopic state [11]:

$$\langle \mathbf{S}^g \rangle = \bar{\mathbf{S}}, \langle \mathbf{D}^g \rangle = \bar{\mathbf{D}}. \tag{14}$$

The inputs of the VPSC model as well as the Taylor ($\mathbf{D}^g = \bar{\mathbf{D}}$) and static ($\mathbf{S}^g = \bar{\mathbf{S}}$) bounds are the slip systems, the initial texture, the microscopic rheological parameters n^s and τ_0^s, and the prescribed macroscopic deformation. On the polycrystal, it is possible to prescribe either the complete macroscopic strain rate $\bar{\mathbf{D}}$, the complete macroscopic stress $\bar{\mathbf{S}}$, but also mixed boundary conditions as discussed below. The numerical convergence of the code is achieved when the relative difference between averaged and barred quantities (equation (14)) is lower than 10^{-4}. This value was found to be small enough to exclude a dependence of model results on any numerical convergence error.

4. DERIVING MICROSCOPIC PARAMETERS

4.1. Method

Prior to applying the VPSC model to polycrystalline ices, the τ_0^s and n^s values of all slip systems must be determined. The slip systems we used to describe ice crystal plasticity are listed in Table 1. Prismatic $\{01\bar{1}0\}\langle 2\bar{1}\bar{1}0\rangle$ slip represents glide of short non-basal edge dislocation segments. Since both basal and prismatic systems together provide only 4 independent systems, we add pyramidal $\{11\bar{2}2\}\langle 11\bar{2}\bar{3}\rangle$ slip, proposed by Hutchinson [27] and Duval *et al.* [25], to permit artificially axial deformation of grains along the c-axis. We denote τ_b, τ_{pr}, and τ_{py} as the RRSS of basal, prismatic, and pyramidal glide, respectively. For the sake of simplicity, we choose the same microscopic stress exponent $n^s = 3$ for all systems.

To determine the RRSS of *in situ* grains, we use an inverse approach. From the literature, we have selected 19 mechanical tests performed on 10 strongly anisotropic polycrystals of polar ice, all samples exhibiting different textures. The deformation of these samples was small enough to impede texture development, but sufficiently large to reach a "steady state" for the viscosity (secondary creep). Thus, for each sample, some components of the viscosity tensor can be determined experimentally. Since each mechanical test was performed on initially annealed samples, one should find, by reproducing experimental tests conditions numerically, at least one set of rheological parameters that reproduces accurately all experimental viscosities.

The textures of samples are shown in Fig. 1. C-axes are either concentrated around the $z'z$ direction (GRIP and Law Dome ices) or in the xz plane (Vostok ices). Vostok samples were deformed under uniaxial compression in the directions $x'x$, $y'y$, and $z'z$, and under biaxial compression in the planes yz, xz, xy [28]. GRIP samples were deformed under uniaxial compression along $z'z$ direction [29], and the Law Dome sample under uniaxial compression along $z'z$, under torsion around $z'z$ and under torsion-compression [30]. Torsion tests on tubular samples are

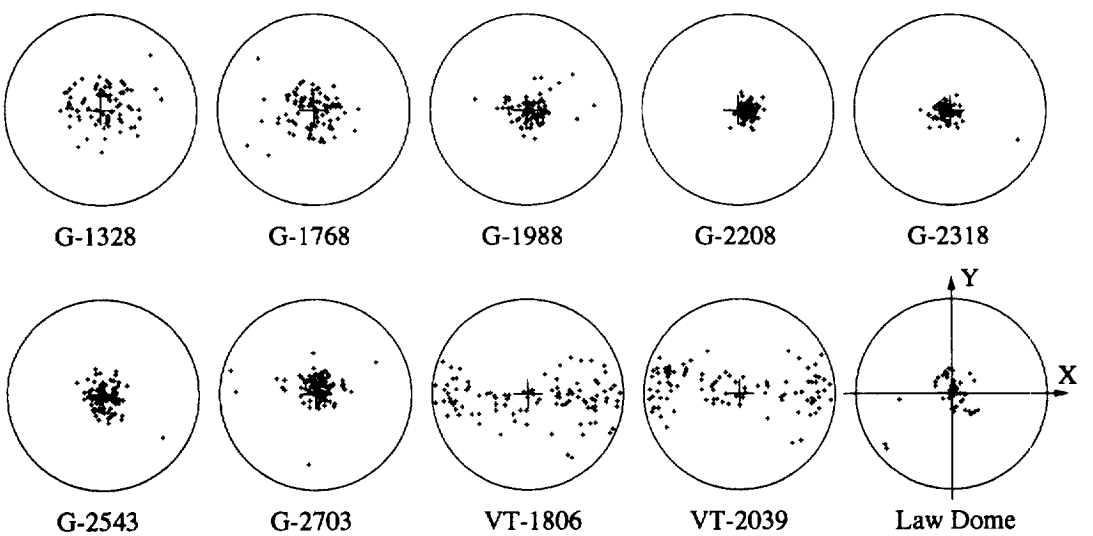

Fig. 1. C-axis textures of GRIP [29], Vostok [5], and Law Dome [30] samples. The centers of Schmid diagrams indicate the *in situ* vertical direction, and the numbers express the *in situ* depth in meters. The axes of the reference frame are shown. Equal-area projection.

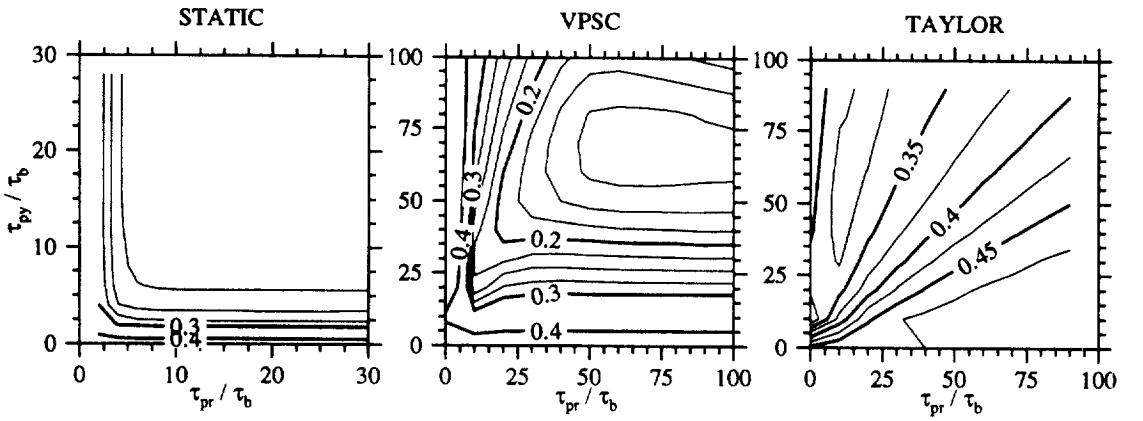

Fig. 2. Average deviation between all 19 mechanical tests and results obtained with the static, VPSC, and Taylor models, as a function of τ_{pr}/τ_b. The interval between thin isovalues is 0.025. Note that scales are different for the static model.

interpreted here as simple shear tests in the xy plane and in the $x'x$ direction.

Ice is assumed to be incompressible, so that stress and strain rate tensors can be expressed as vectors in a 5-D space, using the transformation proposed by Lequeu *et al.* [31]:

$$\mathbf{T} = ((T_{22} - T_{11})/\sqrt{2};\ \sqrt{3/2}T_{33};\ \sqrt{2}T_{23};\ \sqrt{2}T_{13};\ \sqrt{2}T_{12}). \quad (15)$$

We call $\mathbf{T}$ irrespectively the 5-component vector and the second order tensor. To compare all mechanical tests together, we express experimental results for a given value of the macroscopic work rate $\dot{\bar{W}} = \bar{\mathbf{S}}:\bar{\mathbf{D}}$. For doing this, we multiply the macroscopic stress $\bar{\mathbf{S}}$ by a dimensionless factor:

$$k^* = \sqrt{\frac{3}{2}}\left(\frac{\dot{\gamma}_0\sigma_0}{\dot{\bar{W}}}\right)^{1/(n+1)}, \quad (16)$$

and then the macroscopic strain rate $\bar{\mathbf{D}}$ by k^{*n} for homogeneity reasons. We call $\bar{\mathbf{S}}^*$ and $\bar{\mathbf{D}}^*$ the obtained deviatoric stress and strain rate tensors, respectively. The new work rate $\dot{\bar{W}}^*$ reads:

$$\dot{\bar{W}}^* = \bar{\mathbf{S}}^*:\bar{\mathbf{D}}^* = \sqrt{\tfrac{3}{2}}^{n+1}\dot{\gamma}_0\sigma_0. \quad (17)$$

With this transformation, all equipotential surfaces corresponding to the Norton behavior are represented in the 5-D stress space by a unique hypersphere of radius σ_0. Experimental results are not given explicitly here, but some typical behaviours will be presented in detail in Section 5. We find that the norm of $\bar{\mathbf{S}}^{*\text{exp.}}$ vectors lie at $-10°$C between 148 MPa (torsion on the Law Dome sample) and 569 MPa (compression on the GRIP-2543m sample), a variation which is significantly larger than the uncertainty on σ_0. Note also that even if GRIP samples all present similar texture patterns, a clear correlation between texture concentration and directional viscosity is found; the norm of $\bar{\mathbf{S}}^{*\text{exp.}}$ varies between 310 MPa (GRIP-1328m) and 569 MPa (GRIP-2543m).

Calculations are performed using the textures measured on natural samples as input for the models. The deformation conditions prescribed experimentally on each sample were reproduced numerically as accurately as possible. For example, in the case of uniaxial compression along the $z'z$ axis with no friction between apparatus plates and the sample, only $\bar{\mathbf{S}}$ is prescribed numerically. In the case of a biaxial compression test in the $x'x$ and $y'y$ directions, $\bar{D}_{xx}$, $\bar{D}_{yy}$, and $\bar{D}_{xy}$ are prescribed ($\bar{D}_{xy} = 0$) with the conditions $\bar{S}_{xz} = \bar{S}_{yz} = 0$ on shear stresses. Note that $\bar{S}_{xy}$ is not null in general [32], a result which is not consistent with experiments if there is no friction between apparatus plates and the sample. In fact, one can show that biaxial compression tests lead to a non-uniform distribution of normal stresses over the sample surfaces, unless the texture presents particular symmetries. Here, we replace this non-uniform distribution by a uniform shear stress $\bar{S}_{xy}$, and we verified *a posteriori* that $\bar{S}_{xy}$ is small.

We calculate, for each of the 19 mechanical tests and for different values of the RRSS, the deviation between experimental and model results, defined as:

$$\text{deviation} = \left(\frac{(\bar{\mathbf{S}}^{*\text{exp.}} - \bar{\mathbf{S}}^{*\text{mod.}}):(\bar{\mathbf{S}}^{*\text{exp.}} - \bar{\mathbf{S}}^{*\text{mod.}})}{\bar{\mathbf{S}}^{*\text{exp.}}:\bar{\mathbf{S}}^{*\text{exp.}}}\right)^{1/2} \quad (18)$$

This deviation represents the relative distance in the stress space between the point corresponding to $\bar{\mathbf{S}}^{*\text{mod.}}$ and that corresponding to $\bar{\mathbf{S}}^{*\text{exp.}}$. To calculate $\bar{\mathbf{S}}^{*\text{mod.}}$, we adjust τ_b for each couple (τ_{pr}/τ_b; τ_{py}/τ_b) such that the model reproduces the viscosity of an isotropic polycrystal (i.e. the value of σ_0). Note that the VPSC model does not exactly predict a Norton behavior for isotropic polycrystals, indicating a slight sensitivity of isotropic behavior on the third stress invariant. However, this feature is not found to significantly affect our results.

4.2. Results

We estimate that experimental uncertainties can lead to a maximum deviation of about 0.2 for each mechanical test individually. Figure 2 shows the deviation averaged over all 19 mechanical tests. Results have been obtained with the VPSC, Taylor, and static models, and are plotted as functions of τ_{pr}/τ_b and τ_{py}/τ_b. Since some experimental rheologies are expected to be better reproduced than others, a good agreement with individual experiments can be obtained only if this average deviation is significantly lower than 0.2. With the VPSC model, the average deviation presents a minimum value of 0.11 for $\tau_{pr}/\tau_b = \tau_{py}/\tau_b \approx 70$. Therefore, for this model, experimental viscosities can be reproduced *in average* in a satisfactory way. By comparison, static and Taylor models give worse results. The deviation obtained with the static model no longer varies when τ_{pr}/τ_b and τ_{py}/τ_b are both greater than 10; the minimum deviation is about 0.21, i.e. about twice that obtained with the VPSC model. For the Taylor model, the minimum deviation (≈ 0.30), obtained for $\tau_{pr}/\tau_b = 10$ and $\tau_{py}/\tau_b = 50$, is far more than the maximal acceptable value.

These results can be better understood by analyzing the activity (defined as the relative contribution of a particular system to the total deformation) of all slip systems. Average activity, calculated from the 19 mechanical tests, of basal, prismatic, and pyramidal slip systems are presented in Fig. 3. Globally, for each model, the relative activity of a particular system decreases with increasing RRSS. The Taylor model largely underestimates basal activity (≤ 0.45). This result, together with the

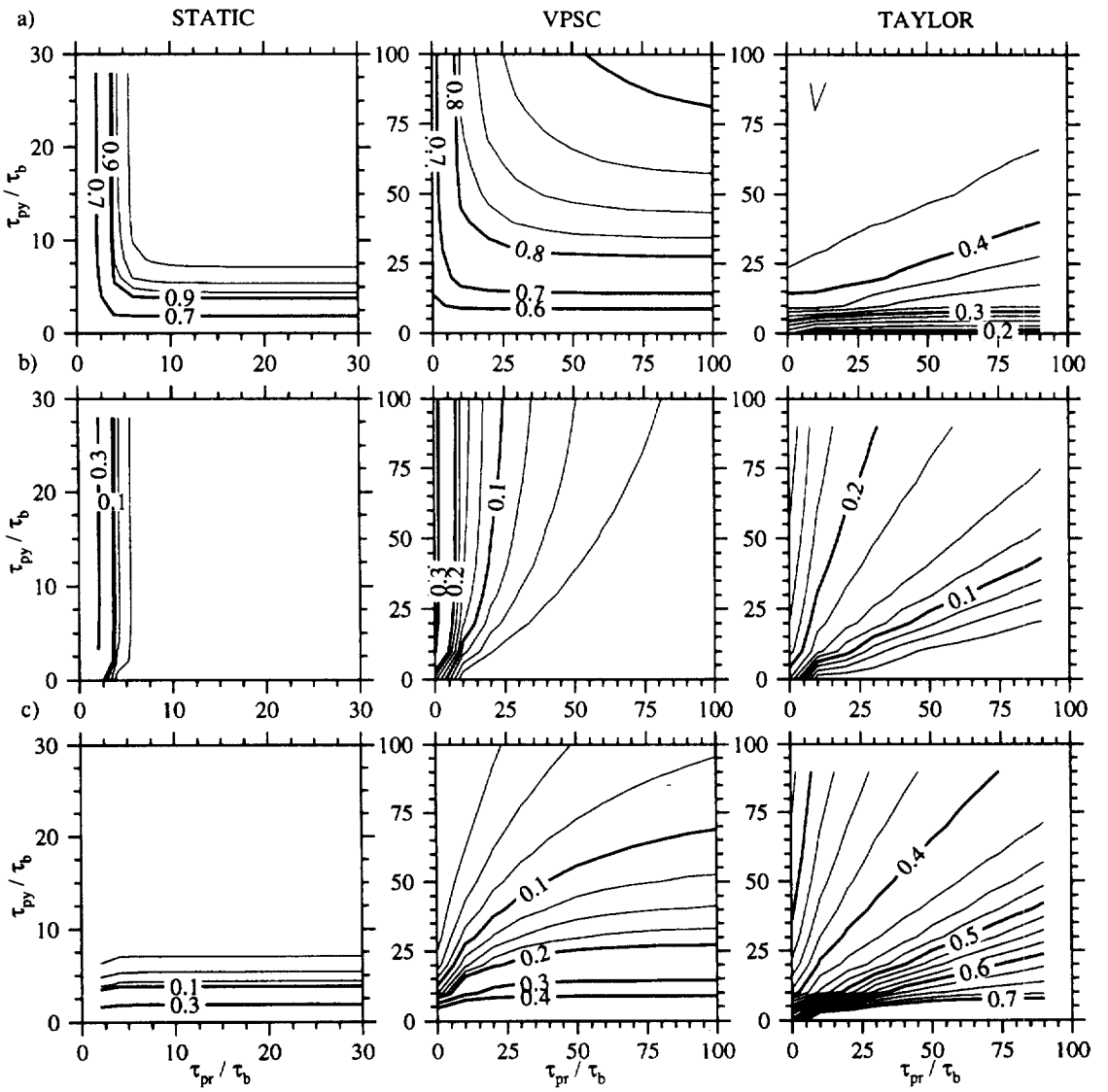

Fig. 3. Average activity of (a) basal, (b) prismatic, and (c) pyramidal slip systems, calculated with static, VPSC, and Taylor models as a function of τ_{pr}/τ_b and τ_{py}/τ_b. The interval between thin isovalues is 0.025.

Table 2. RRSS values, expressed in MPa, obtained with the static, VPSC, and Taylor models, corresponding to $\tau_{pr}/\tau_b = \tau_{py}/\tau_b = 70$

	Static	VPSC	Taylor
τ_b	71.5	7.76	2.49
τ_{pr}	5005	543	174
τ_{py}	5005	543	174

large value of the minimum average deviation, shows that this model cannot be realistically applied to polycrystalline ice, whatever the set of RRSS we choose. With the static model, the comparison of Figs 2 and 3 shows that the best estimation of polycrystal behaviour is obtained when the basal activity is maximum, i.e. for $\tau_{pr}/\tau_b \geq 10$ and $\tau_{py}/\tau_b \geq 10$. This is in accordance with the intuitive idea that since non-basal dislocations are rarely observed, non-basal slip could be omitted in the simulations. But interestingly, a different feature is found for the VPSC model. Indeed, basal activity increases with non-basal RRSS, but the average deviation is not minimum for maximum non-basal RRSS. Within the VPSC model, it is thus necessary to introduce a certain amount of non-basal activity to accurately reproduce experimental results. For $\tau_{pr}/\tau_b = \tau_{py}/\tau_b = 70$, basal and prismatic activities (respectively 0.89 and 0.02) are physically acceptable. Pyramidal activity remains small (≈ 0.09), but the occurrence of such a deformation mechanism has never been demonstrated experimentally. This set of RRSS thus leads to the best reproduction of experimental macroscopic behavior with realistic active deformation mechanisms except for pyramidal slip. One can also choose to reduce as much as possible the pyramidal slip by selecting a set of RRSS that leads to worse (but still acceptable) prediction of macroscopic behaviors, for example $\tau_{pr}/\tau_b = 50$ and $\tau_{py}/\tau_b = 90$. In that case, the pyramidal activity (≈ 0.06) is still not negligeable. In fact, one should retain that pyramidal slip cannot be completely suppressed, even if the numerical convergence can be achieved with basal slip only [14].

In the following, we will use the set $\tau_{pr}/\tau_b = \tau_{py}/\tau_b = 70$ for all models. It provides the best accordance with experiments for both VPSC and static models, but not for the Taylor model; this (unrealistic) upper bound will be applied only to better understand the influence of model assumptions on results. We get the values of τ_b, τ_{pr}, and τ_{py} by adjusting τ_b in order to reproduce the value of σ_0 for an isotropic polycrystal, see Table 2. Accordingly, values of RRSS largely depend on model assumptions. We find, for example, that τ_b obtained with the static model is 10 times as large as that obtained with the VPSC model. We can also compare these results with values of RRSS obtained to reproduce the experimental behaviour of *isolated* single crystals given by Duval *et al.* [25]:

$$5 \leq \tau_b \leq 22 \text{ MPa}, \quad \tau_{pr} \geq 297 \text{ MPa}, \quad \tau_{py} \geq 429 \text{ MPa}. \tag{19}$$

The VPSC estimation of the rheology of *in situ* grains well matches that obtained experimentally on isolated single crystals. A similar feature was found by Lebensohn and Tomé on zirconium [13]. This tends to indicate that the structure of grain boundaries should not significantly affect the macroscopic behavior of ice polycrystals.

4.3. *Effects of strength of interaction*

We have used a VPSC approach to calculate the behaviour of grains within a polycrystal, by comparing experimental instantaneous responses of 10 strongly anisotropic samples with those determined numerically for various sets of basal, prismatic, and pyramidal resistance. We have shown the very good agreement between experiments and average predictions of the VPSC model for the macroscopic flow stress. On the other hand, the Taylor model can be completely disregarded for polycrystalline ice. The VPSC estimation of RRSS is in very good accordance with experiments on isolated single crystals, but very large variations are found between VPSC, static, and Taylor estimations of RRSS.

At this point, it is worthwhile to look at the sensitivity of results on the assumptions of the "1-site" VPSC formulation. A simple test consists of introducing, in the interaction equation (10), an interaction coefficient α [33]:

$$\mathbf{D}^g - \bar{\mathbf{D}} = -\alpha \times \tilde{\mathbf{M}}:(\mathbf{S}^g - \bar{\mathbf{S}}) \tag{20}$$

which is used to constrain the interaction between grains and the HEM. A zero value of α corresponds to the Taylor model, a value of unity to the *tangent* VPSC model used here, and an infinite value to the static model. The evolution of the relative flow stress σ_0/τ_b of an isotropic polycrystal with α is plotted in Fig. 4, for $\tau_{pr}/\tau_b = \tau_{py}/\tau_b = 70$. According to Tóth *et al.* [34] and Molinari and Tóth [33], the real behavior of polycrystals should lie between the VPSC *secant* approach ($\alpha = 1/n$), corresponding to the incremental model of Hutchinson [11], and the VPSC *tangent* approach ($\alpha = 1$). With the secant model, we find a value of σ_0/τ_b as large as 2.8 times that obtained with the tangent model, and a basal activity of only 0.52 for isotopic polycrystals instead of 0.98 for the tangent model. In order to have a more realistic (i.e. larger) basal activity with the secant model, it is thus necessary to impose τ_{pr}/τ_b and τ_{py}/τ_b significantly larger than 70. As a result, we see that to reproduce the experimental behavior of anisotropic polycrystals, we should choose RRSS values that are signficiantly different than those given in Table 2. Since the secant model is closer to the Taylor model, it can probably not reproduce macroscopic behavior as accurately as the tangent model.

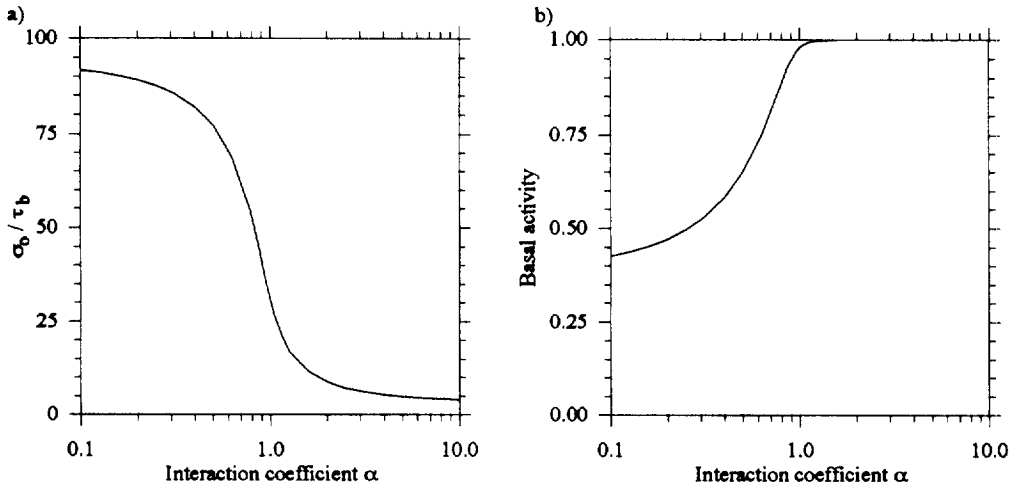

Fig. 4. Sensitivity of (a) the macroscopic relative flow stress and (b) the basal activity on the interaction coefficient α, for an isotropic polycrystal and taking $\tau_{pr}/\tau_b = \tau_{py}/\tau_b = 70$.

Microscopic parameters are thus found to be very sensitive to model assumptions, and the VPSC estimation of RRSS should be considered only as a first approximation of real values.

4.4. *About work rate conservation*

We now concentrate on another simple test, which consists of checking if the work rate is conserved, i.e. if the macroscopic work rate $\bar{\mathbf{S}}:\bar{\mathbf{D}}$ equals the mean microscopic work rate $\langle \mathbf{S}^g:\mathbf{D}^g \rangle$. Figure 5(a) shows the relative difference between these work rates, for an isotropic polycrystal, as a function of τ_b/τ_{pr} and for $\tau_{py} = \tau_{pr}$. If the VPSC model could allow the calculation of a stress field that is in equilibrium everywhere in the polycrystal, then this difference would vanish. However, the VPSC model treats the case of a population of inclusions, each of which is in equilibrium with the HEM, but without constraining the equilibrium between them. The difference between work rates can be expressed in quadratic form:

$$\bar{\mathbf{S}}:\bar{\mathbf{D}} - \langle \mathbf{S}^g:\mathbf{D}^g \rangle = \langle (\mathbf{S}^g - \bar{\mathbf{S}}):\bar{\mathbf{M}}:(\mathbf{S}^g - \bar{\mathbf{S}}) \rangle \quad (21)$$

which is not null in general and which is found to increase with the microscopic anisotropy. Such a discrepancy between macroscopic and averaged microscopic dissipated (and/or stored) energies (and/or work rate) is expected for all kinds of "1-site" self-consistent schemes relying on an interaction equation (elastic, elastoplastic, . . .). Here, the relative difference between work rates is maximum for the tangent approach (Fig. 5(b)) and a value as high as 6.0 is attained for $\tau_{pr}/\tau_b = \tau_{py}/\tau_b = 70$. Such a high value indicates that the simplifications of the "1-site" VPSC formulation leads to significant inaccuracy for strongly anisotropic materials like ice. Three major simplifications are introduced in the "1-site" scheme:

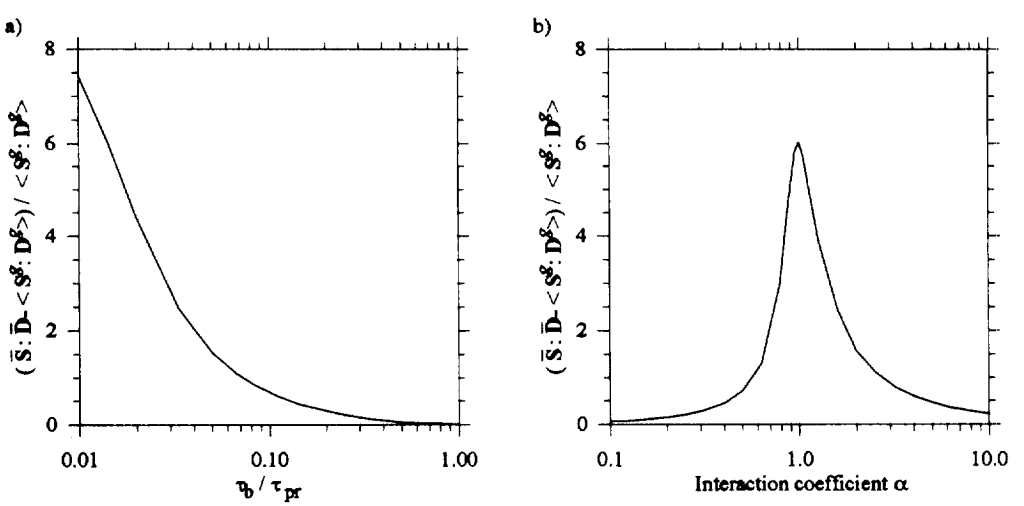

Fig. 5. Relative difference between the macroscopic work rate and the mean microscopic work rate, calculated with the VPSC model for an isotropic polycrystal. (a) $\tau_{pr} = \tau_{py}$, $\alpha = 1$; (b) $\tau_{pr}/\tau_b = \tau_{py}/\tau_b = 70$.

1. The stress and deformation states are assumed to be uniform in each grain, which is only a rough estimation of natural deformations [35, 36].
2. Topological effects, which have a significant influence on local states [37–39], are not taken into account.
3. The behavior of the HEM is linearized in the vicinity of the prescribed stress. According to Gilormini [40], the VPSC model extended to non-linear materials may lead in certain cases to a macroscopic behavior that violates the more restrictive upper bound of Ponte Castañeda.

Accordingly, the VPSC model cannot be used to evaluate stress or deformation in a particular grain, but only to estimate *average* stress or deformation of grains having a particular orientation. The influence of the linearization of the HEM behavior is more difficult to analyze, but it is clear that it introduces an error that increases with the non-linearity of the macroscopic behavior and with the microscopic anisotropy since this anisotropy introduces stress concentrations.

This analysis indicates that the application of the VPSC model to non-linear strongly anisotropic materials requires some precautions. We have shown that our VPSC estimates of RRSS must be taken only as a rough approximation of real values. In particular, the strong dependence of RRSS values on model assumptions limits the physical interpretations of our results. If τ_b is theoretically linked to the density and the mobility of basal dislocations, the value of τ_{py} has less physical meaning since pyramidal slip has never been clearly observed in ice. Here, pyramidal slip provides one additional degree of freedom and permits axial deformation along c-axes. One possibility is that the artificial introduction of this slip system is necessary to correct, in some way, the errors linked to the simplifications of the "1-site" VPSC approach.

5. ANISOTROPIC BEHAVIOR

We will now use the VPSC model to highlight some features of anisotropic ice behavior. We focus here on two particular samples, VT2039 and Law Dome, since both of these samples have been subjected to several mechanical tests (5 and 3, respectively). The behaviors described below nevertheless hold also for VT1806 and GRIP samples. The VT2039 sample was deformed experimentally under uniaxial compression (points A and B in Fig. 6) and biaxial compression (C, D, E). The Law Dome sample was deformed under uniaxial compression (F), torsion (G), and torsion–compression (H).

Micro–macro models can be used to describe polycrystal behavior by calculating an equi-work-rate surface in the 5-D stress space. Figure 6(a) shows a projection on the deviatoric plane $\{\bar{S}_1^*, \bar{S}_2^*\}$ of the surface calculated for the VT2039 sample with VPSC, Taylor, and static models. The plane projection of the 5-D surface, as defined by Canova *et al.* [32], is calculated by prescribing $\bar{D}_3^* = \bar{D}_4^* = \bar{D}_5^* = 0$. Note that these conditions do not correspond to deformation conditions of uniaxial and biaxial compression, as discussed in Section 4.1. However, sections and projections of equi-work-rate surfaces corresponding to experimental deformation conditions are almost superimposed on the projection of Fig. 6(a), and are thus not shown here. We find that maximum values of shear stresses $\bar{S}_3^*$, $\bar{S}_4^*$, and $\bar{S}_5^*$ never exceed 20% of the maximum axial stresses $\bar{S}_1^*$ and $\bar{S}_2^*$. This indicates that for the VT2039 sample, the deviatoric plane $\{\bar{S}_1^*, \bar{S}_2^*\}$ is nearly closed, i.e. that axial stresses mainly induce axial deformations, and vice-versa [32]. This fact is in accordance with the nearly plane symmetry, around xz, of the c-axes texture. This remark is important. Indeed, we have shown in Section 4.1 that biaxial compression tests on natural samples, for which textures always present a slight asymmetry, necessarily induce a non-uniform distribution of axial stresses on sample surfaces. But since the deviatoric plane is found to be nearly closed, this non-uniformity is expected to remain small. Therefore, biaxial tests on the VT2039 samples are valid.

Equi-work-rate surfaces indicate the resistance of the sample with respect to any stress direction. A good agreement with experimental data is found for the VPSC model. Individually, *each* experimental behavior is reproduced numerically. Less accurate results are obtained with static and Taylor models, as previously seen in Fig. 2.

Let us now define a macroscopic stress potential $\bar{\phi}$, such that:

$$\bar{D}_{ij} = \frac{\partial \bar{\phi}}{\partial \bar{S}_{ij}}. \tag{22}$$

In the 5-D stress space, the strain rate vector $\bar{\mathbf{D}}$ is normal to the equipotential surface corresponding to the prescribed stress $\bar{\mathbf{S}}$. The VPSC surface of Fig. 6(a) presents two sharp edges which, if found on an equipotential instead of an equi-work surface, could lead to an instable viscoplastic behavior. According to Hutchinson [11], the particular form of the microscopic constitutive relation (4) leads to an unusually simple connection between macroscopic potential and macroscopic work rate:

$$\bar{\phi} = \frac{\dot{\bar{W}}}{n+1} \tag{23}$$

if $\bar{\mathbf{S}}:\bar{\mathbf{D}} = \langle \mathbf{S}^g:\mathbf{D}^g \rangle$. This is for example the case for the static and Taylor models. Therefore, equi-work-rate surfaces calculated with these models are also equipotentials, and the normality rule thus holds for equi-work-rate surfaces. However, as shown previously, the condition $\bar{\mathbf{S}}:\bar{\mathbf{D}} = \langle \mathbf{S}^g:\mathbf{D}^g \rangle$ is not verified for the VPSC model. As a result, the relation (23) is not necessarily valid, i.e. $\dot{\bar{W}}$ is not necessarily

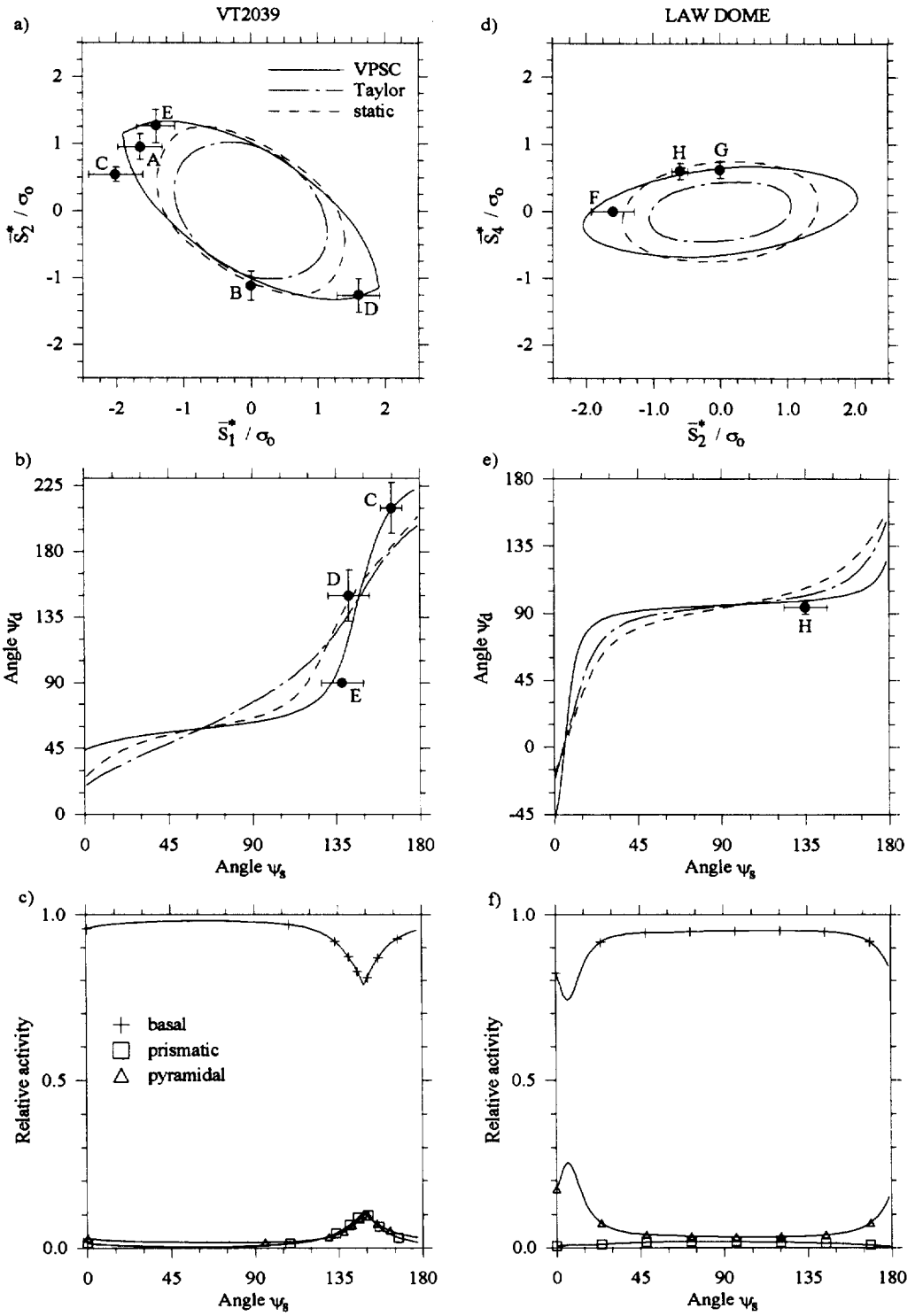

Fig. 6. Rheology of VT2039 (a, b, c) and Law Dome (d, e, f) samples, calculated with VPSC, Taylor, and static models, compared to experimental data. (a) projection of the equi-work-rate surfaces on the deviatoric plane and (d) section by the $\{\bar{S}_2^*, \bar{S}_4^*\}$ subspace. (b, e) relation between the orientation ψ_d of vector $\bar{\mathbf{D}}$ and the orientation ψ_s of $\bar{\mathbf{S}}$. (c, f) relative activity of basal, prismatic, and pyramidal systems predicted by the VPSC model.

proportional to $\bar{\phi}$, and the normality rule does not necessarily hold for VPSC equi-work-rate surfaces.

One way to describe in more detail how the orientation of $\bar{\mathbf{D}}$ varies with that of $\bar{\mathbf{S}}$ is to plot the angle ψ_d between vector $\bar{\mathbf{D}}$ and the x-axis (here the $\bar{S}_1^*$-axis) as a function of the angle ψ_s between vector

$\bar{\mathbf{S}}$ and the x-axis, as in Fig. 6(b). Note that for the VPSC model, we find again a very good agrement with the experimental points C, D, E. Here, points A and B cannot be plotted, since the direction of $\bar{\mathbf{D}}$ was not completely determined experimentally. The behavior of the VT2039 sample can be decomposed into two distinct domains. The first corresponds to $0° \leq \psi_s \leq 120°$, for which ψ_d is only slightly sensitive to ψ_s. In this domain, a variation of the stress vector direction of 120° causes a variation of the strain rate vector direction of only 30°. The direction of $\bar{\mathbf{D}}$ is very "stable". The second domain, which exhibits the opposite behaviour, corresponds to $120° \leq \psi_s \leq 180°$ i.e. to the vicinity of the edges. Here, the direction of $\bar{\mathbf{D}}$ is very sensitive to that of $\bar{\mathbf{S}}$. According to Fig. 6(c), a sharp minimum of basal activity is found in this domain. A large amount of non-basal slip then renders the direction of $\bar{\mathbf{D}}$ very sensitive to that of $\bar{\mathbf{S}}$. At $\psi_s = 148°$, i.e. for the edges, prismatic and pyramidal activities both reach a value of about 0.1. Especially for pyramidal slip, the realism of such a relatively high value can be questioned, despite the very good agreement between modelled behavior and experiments.

The behavior of the Law Dome sample presents an overall similar behavior, but with one important difference. Figure 6(d) shows the sections of the equi-work-rate surfaces by the $\{\bar{S}_2^*, \bar{S}_4^*\}$ plane, calculated with VPSC, static, and Taylor models. These sections are obtained by prescribing $\bar{S}_1^* = \bar{S}_3^* = \bar{S}_5^* = 0$. A very good agreement with *all* experiments is obtained with the VPSC model, whereas the static model also gives satisfactory results here. Similarly to the VT2039 sample, two distinct behaviors are observed. When the equi-work-rate surface presents a small curvature, i.e. for $-15° \leq \psi_s \leq 30°$, a smaller contribution of basal slip is found, and the strain rate direction is very sensitive to the stress direction (Fig. 6(e) and (f)). Here again, pyramidal activity (max. = 0.25) is far larger than expected.

The c-axes texture of the law Dome sample is nearly axisymmetrical about the $z'z$ axis. Intuitively, we expect the $\{\bar{S}_1^*, \bar{S}_2^*\}$ and $\{\bar{S}_4^*\}$ subspaces to be nearly closed. In fact, this is not the case at all. For example, during a compression creep test in the $z'z$ direction, i.e. for $\bar{\mathbf{S}} = (0, \bar{S}_2^*, 0, 0, 0)$ and $\psi_s = 180°$, the VPSC model predicts $\psi_d = 131°$. A shear strain rate $\bar{D}_4^*$ then appears, and its absolute value is close to that of $\bar{D}_2^*$. Thus, axial stresses also induce a significant shear strain rate. A similar feature appears for shear deformation. If the strain rate $\bar{\mathbf{D}} = (0, 0, 0, \bar{D}_4^*, 0)$ is prescribed, i.e. $\psi_d = 90°$, then $\psi_s = 37°$ according to the VPSC model. In this case, a significant tensile stress $\bar{S}_2^*$ appears in the sample. For the Law Dome sample, the apparent symmetry of the texture does not allow us to conclude directly if specific subspaces are closed. This last point is important for the interpretation of mechanical tests. In ice sheets, deep ice is mainly deformed by shear parallel to the xy plane. The shear viscosity of samples with a similar texture as our Law Dome sample is thus of great importance for calculating and interpreting the large scale flow of polar ices. However, the value of this viscosity component is still subjected to discussion. For example, Lile [41] and Russel-Head and Budd [42] have found a relatively large viscosity by performing shear tests with a constant distance between apparatus plates, i.e. by prescribing $\bar{D}_2^* = 0$ and thus $\psi_d = 90°$ in Fig. 6(d). Legac [30] has found a much lower viscosity for a very similar sample, but with an apparatus allowing free axial deformation of the sample, i.e. under the conditions $\psi_s = 0°$ leading to $\psi_d \neq 90°$. These two deformation conditions are very different. In Lile's and in Russel-Head and Budd's experiments, a large axial stress $\bar{S}_2^*$ appears, while in Legac's experiments, a small axial strain rate $\bar{D}_2^*$ occurs. The results of these different authors therefore cannot be directly compared. When applying the VPSC model to Legac's experiments, we obtain a smaller value of $\bar{S}_4^*$, corresponding to a lower shear viscosity.

6. CONCLUSION

We have applied a ViscoPlastic Self-Consistent (VPSC) model to characterize the instantaneous anisotropic behavior of textured polycrystalline ice. Ice crystals were assumed to deform by dislocation glide on basal, prismatic, and pyramidal planes. Results were compared to those obtained with Taylor and static bounds. We have used an inverse method to derive the microscopic parameters of the models. This method is based on the comparison between model results and anisotropic macroscopic behavior measured experimentally. It permits us to determine *all* sets of microscopic parameters usable for the simulations. We have found that the best VPSC estimate of the behavior of grains embedded in a polycrystal is similar to the one determined experimentally on isolated monocrystals. However, the calculated resistances of slip systems are found to be very sensitive to model assumptions.

The VPSC model reproduces very well the macroscopic behavior of strongly textured samples. We show however that this good agreement cannot be obtained without the introduction of a relatively small—but not negligible—amount of pyramidal slip, which is not observed experimentally. The introduction of this probably unrealistic slip system, which provides one additional degree of freedom for the microscopic deformations, cannot be interpreted from the physical point of view. Indeed, the plastic work is far from conserved within the "1-site" VPSC approach when the material presents a strong anisotropy (like ice), indicating that the mechanical equations are only very roughly solved in the polycrystal. This discrepancy is to be expected for all kinds of "1-site" self-consistent schemes relying on an interaction equation. As a result, the normality rule

does not necessarily hold for VPSC equi-work-rate surfaces.

We have finally analyzed the relation between texture symmetries and macroscopic behavior. Textured ice samples always tend to deform in a direction that favours basal slip. However, for polar ices, closed subspaces as defined by Canova *et al.* [32] for ideal textures cannot be directly determined from natural texture patterns. Since polar ices are subjected to a complex *in situ* deformation history, textures never present perfect symmetries. In certain cases, subspaces which are closed for an ideally symmetric texture are far from closed when the texture is only nearly symmetric. This should be taken into account to improve future mechanical test conditions and to interpret *in situ* field measurements.

Acknowledgements—This work was supported by the PNEDC (Programme National d'étude de la Dynamique du Climat) CNRS, and by the CEC (Commission of European Communities) Environment Program.

REFERENCES

1. Li, J., Interrelation between flow properties and crystal structure of snow and ice. Ph.D. thesis, University of Melbourne, Australia, 1994.
2. Thorsteinsson, Th., Kipfsuhl, J. and Miller, H., *J. Geophys. Res.*, 1996, in press.
3. Lipenkov, V. Ya., Barkov N. I., Duval, P. and Pimienta, P., *J. Glaciol.*, 1989, **35**(121), 392.
4. Shoji, H. and Langway, C. C., in *Geophysical Monograph*, Vol. 33. American Geophysical Union, Washington DC, 1985, pp. 39–48.
5. Pimienta, P., Duval, P. and Lipenkov, V. Y., in *The Physical Basis of Ice Sheet Modelling*. International Association of Hydrological Sciences, Vancouver, 1987, Publication 170, pp. 57–66.
6. Budd, W. F. and Jacka, T. H., *Cold Reg. Sci. technol.*, 1989, **16,** 107.
7. Mangeney, A., Modélisatoin de l'écoulement de la glace dans les calottes polaires: prise en compte d'une loi de comportement anisotrope. Ph.D. thesis, Université Pierre et Marie Curie (Paris VI), France, 1996.
8. Mangeney, A., Califano, F. and Castelnau, O., *J. Geophys. Res.*, 1996, in press.
9. Lliboutry, L., *Int. J. Plasticity.*, 1993, **9,** 619.
10. Svendsen, B. and Hutter, K., *Ann. Glaciol.*, 1996, **23,** 262.
11. Hutchinson, J. W., *Proc. R. Soc. Lond.*, 1976, **A348,** 101.
12. Molinari, A., Canova, G. R. and Ahzi, S., *Acta metall.*, 1987, **35**(12), 2983.
13. Lebensohn, R. A. and Tomé, C. N., *Acta metall.*, 1993, **41**(9), 2611.
14. Castelnau, O., Duval, P., Lebensohn, R. A. and Canova, G. R., *J. Geophys. Res.*, 1996, **101**(B6), 13851.
15. Castelnau, O., Thorsteinsson, Th., Kipfstuhl, J., Duval, P. and Canova, G. R., *Ann. Glaciol.*, 1996, **23,** 194.
16. Muguruma, J., *Brit. J. Appl. Phys. (J. Phys. D)*, 1969, **2**(2), 1517.
17. Mercier, S., Tóth, L. S. and Molinari, A., *Textures and Microstructures*, 1995, **25,** 45.
18. Tóth, L. S. and Serghat, M., *Textures and Microstructures*, 1996, **26–27,** 221.
19. Fukuda, A. T., Hondoh T. and Higashi, A., *J. Physique*, 1987, **48,** Col. C1(suppl. 3), 163.
20. Hondoh, T., Iwamatsu, H. and Mae, S., *Phil. Mag.*, 1990, **A62**(1), 89.
21. Higashi, A., Fukuda, A., Hondoh, T., Goto, K. and Amakai, S., in *Proc. Yamada Conf. IX on Dislocations in Solids*, T. Suzuki, T. Ninomiya, K. Sumino, and S. Takeuchi, eds., University of Tokyo Press, Tokyo, 1985, pp. 511–515.
22. Shearwood, C. and Whitworth, R. W., *J. Glaciol.*, 1989, **35**(120), 281.
23. Ahmad, S. S. and Whitworth, R. W., *Phil. Mag.*, 1988, **A57**(5), 749.
24. Petrenko, V. F. and Whitworth, R. W., Structure of ordinary ice Ih, Part II: Defects in ice, Vol. 2: Dislocations and plane defects. Technical Report 94-12, CRREL, 1994.
25. Duval, P., Ashby M. F. and Anderman, I., *J. Phys. Chem.*, 1983, **87**(21), 4066.
26. Eshelby, J. D., *Proc. R. Soc. Lond.*, 1957, **A241,** 376.
27. Hutchinson, J. W., *Metall. Trans.*, 1977, **8A**(9), 1465.
28. Pimienta, P., Etude du comportement mécanique des glaces polycristallines aux faibles contraintes; applications aux glaces des calottes polaires. Ph.D. thesis, Université Scientifique et Médicale de Grenoble, France, 1987.
29. Milsch, H., Mechanishches Verhalten von Eis langs des Bohrkerns aus dem Greenland Ice core Project (GRIP) in Relation zur praferentiellen Gitterorientierung der Eiskristalle. Diplomarbeit, Georg-August-Universitat, Gottingen, Germany, 1994.
30. Legac, H., Contribution à la détermination des lois de comportement de la glace polycristalline (anélasticité et plasticité). Ph.D. thesis, Université Scientifique et Médicale de Grenoble, France, 1980.
31. Lequeu, Ph., Gilormini, P., Montheillet, F., Bacroix B. and Jonas, J. J., *Acta metall.*, 1987, **35**(2), 439.
32. Canova, G. R., Kocks, U. F., Tomé, C. N. and Jonas, J. J., *J. Mech. Phys. Solids.*, 1985, **33**(4), 371.
33. Molinari, A. and Tóth, L. S., *Acta metall. mater.*, 1994, **42**(7), 2453.
34. Tóth, L. S., Molinari, A. and Bons, P. D., *Mater. Sci. Engin.*, 1994, **A175,** 231.
35. Barber, D. J., Wenk, H. R. and Heard, H. C., *Mater. Sci. Engin.*, 1994, **A175,** 83.
36. Azuma, N., *Cold Reg. Sci. technol.*, 1995, **23,** 137.
37. Wilson, C. J. L. and Zhang, Y., *J. Glaciol*, 1994, **40**(134), 46.
38. Becker, R. and Panchanadeeswaran, S., *Acta metall. mater.*, 1995, **43**(7), 2701.
39. Sarma, G. B. and Dawson, P. R., *Acta mater.*, 1996, **44**(5), 1937.
40. Gilormini, P., *Proc. IUTAM Symp. on Micromechanics of Plasticity and Damage of Multiphase Materials*, Sèvres (France), 29 August–1 September 1995, Kluwer Academic Publishers, Dordrecht.
41. Lile, R. C., *J. Glaciol.*, 1978, **21**(85), 475.
42. Russell-Head, D. S. and Budd, W. F., *J. Glaciol.*, 1979, **24**(90), 117.